UC Santa Barbara

Title
Long-range electrostatic screening in ionic liquids

Permalink
https://escholarship.org/uc/item/43d6b6w5

Journal
Proceedings of the National Academy of Sciences of the United States of America, 112(24)

ISSN
0027-8424

Authors
Gebbie, Matthew A
Dobbs, Howard A
Valtiner, Markus
et al.

Publication Date
2015-06-16

DOI
10.1073/pnas.1508366112

Peer reviewed

Long-range electrostatic screening in ionic liquids

Matthew A. Gebbie[a], Howard A. Dobbs[b], Markus Valtiner[c], and Jacob N. Israelachvili[a,b,1]

[a]Materials Department, University of California, Santa Barbara, CA 93106; [b]Department of Chemical Engineering, University of California, Santa Barbara, CA 93106; and [c]Interface Chemistry and Surface Engineering, Max Planck Institut für Eisenforschung GmbH, 40237 Düsseldorf, Germany

Electrolyte solutions with high concentrations of ions are prevalent in biological systems and energy storage technologies. Nevertheless, the high interaction free energy and long-range nature of electrostatic interactions makes the development of a general conceptual picture of concentrated electrolytes a significant challenge. In this work, we study ionic liquids, single-component liquids composed solely of ions, in an attempt to provide a novel perspective on electrostatic screening in very high concentration (nonideal) electrolytes. We use temperature-dependent surface force measurements to demonstrate that the long-range, exponentially decaying diffuse double-layer forces observed across ionic liquids exhibit a pronounced temperature dependence: Increasing the temperature decreases the measured exponential (Debye) decay length, implying an increase in the thermally driven effective free-ion concentration in the bulk ionic liquids. We use our quantitative results to propose a general model of long-range electrostatic screening in ionic liquids, where thermally activated charge fluctuations, either free ions or correlated domains (quasiparticles), take on the role of ions in traditional dilute electrolyte solutions. This picture represents a crucial step toward resolving several inconsistencies surrounding electrostatic screening and charge transport in ionic liquids that have impeded progress within the interdisciplinary ionic liquids community. More broadly, our work provides a previously unidentified way of envisioning highly concentrated electrolytes, with implications for diverse areas of inquiry, ranging from designing electrochemical devices to rationalizing electrostatic interactions in biological systems.

electrostatic interactions | intermolecular interactions | interfacial phenomena | Boltzmann distribution | activation energy

Electrolyte solutions are multicomponent liquids that are composed of ions (solutes) dissolved in a liquid phase (solvent), a classic example being salt water. Like any ideal mixture, the driving force for the dissolution of ions in electrolyte solutions is entropic. Unlike ideal mixtures, the long-range nature and high interaction free energy of the electrostatic interactions between ions ensures that the physical properties of all but the most dilute electrolyte solutions exhibit pronounced deviations from ideal behavior. These deviations primarily arise from the steric "crowding" of ions and the electrostatic correlation of ions, for example the formation of neutral ion pairs, both of which increase the range of electrostatic interactions, compared with ideal solutions (1). As a result, the development of a general conceptual picture of concentrated electrolyte solutions remains challenging. Nevertheless, electrolytes with high ionic concentrations are prevalent in biological systems (2) and technological applications, such as energy storage devices (3–5), so overcoming this challenge remains an important task.

In this work, we study room-temperature ionic liquids (RTILs), single-component liquids composed solely of ions, in an attempt to provide a starting point for a new conceptual understanding of electrostatic screening in concentrated electrolytes. Although RTILs do not have neutral solvent molecules separating the constituent ions, the high degrees of ion crowding and electrostatic correlations present in RTILs are expected to be fundamentally related to ion crowding and electrostatic correlations in highly concentrated electrolyte solutions (5). To date, thousands of RTILs have been identified with diverse physical properties that can be tuned via careful design of cation–anion

pairs (6). Although these properties are largely governed by the same strong coulombic interactions that underlie the 801 °C melting point of crystalline sodium chloride at atmospheric pressure, the large sizes and asymmetric charge distributions of RTIL ions suppress the formation of ordered crystals. Notably, the high thermal and electrochemical stabilities, negligible volatilities, and variable intrinsic ionic conductivities of many RTILs make them promising materials for numerous applications, including electric double-layer capacitors, batteries, and self-assembly media (3–10). Many of these applications depend critically on interfaces between charged surfaces and RTILs. Nevertheless, the fundamental characteristics of RTIL electric double layers remain an active area of research and discussion (5, 11).

A generally accepted picture is that the electric double layers formed by RTILs consist of ordered layers of cations and anions, with these perturbed ionic concentrations quickly approaching bulk distributions on the order of several ionic diameters (5). Much of this understanding was developed through nanoscale computational studies of coarse-grained ionic systems (5, 11–16) that are reminiscent of high-temperature molten salts. These studies predict that the electric double layers formed by RTILs should be short-range and exhibit pronounced charge density oscillations, similar to the screening behavior identified in pioneering work on molten KCl (15). Recent theoretical studies emphasize that complex ion ordering in RTILs can intimately depend on the electrochemical potentials of the charged surfaces (5, 17–19), but these studies have left intact the picture that the electric double layers formed by RTILs should be very short-ranged.

Experimentally, the short-range, surface-induced ordering of ions in RTILs has been confirmed with X-ray scattering experiments, atomic force microscopy (AFM) force measurements, and surface forces apparatus (SFA) measurements (17, 20–23), with these studies highlighting that the ordering of RTIL ions at surfaces exhibits many subtleties. For example, Atkin et al. (22) used AFM to demonstrate that gold electrode surfaces immersed

Significance

Liquid solutions with high concentrations of electrically charged ions are key elements of many energy storage technologies and are prevalent in biology. Nevertheless, they remain poorly understood. We study ionic liquids—liquids composed solely of ions—with the goal of providing a general picture of concentrated ionic solutions. Using molecular-scale experiments, we show that, surprisingly, less than 0.1% of the ions in ionic liquids are "free" to contribute to electrostatic screening, with the remainder "stuck" as neutral aggregates. Our temperature-dependent results provide fundamental guidance for designing high-performance ionic liquids for numerous applications. More broadly, we provide a novel way of envisioning concentrated ionic solutions with wide-ranging implications, such as elucidating the nanoscale properties of underwater bioadhesives and other self-assembled biomolecules.
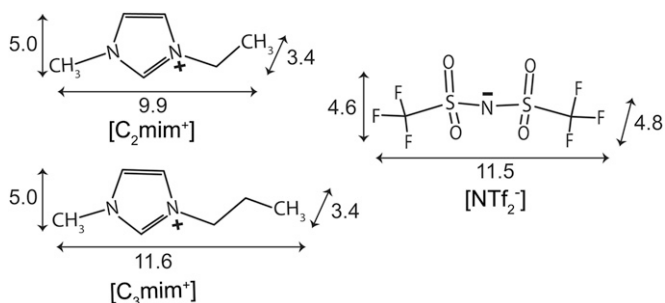
Fig. 1. Chemical structures and approximate dimensions of the RTIL ions. Molecular dimensions in angstroms were calculated from the van der Waals radii of the constituent atoms.

in RTILs can undergo ion-mediated surface reconstructions under externally applied electrochemical potentials. Perkin et al. (23) have shown that RTIL ions self-assemble into ordered (smectic-like) bilayers when the cations contain pronounced nonpolar domains. Recent SFA measurements have added to these pictures by demonstrating the presence of a long-range monotonic, exponentially decaying, equilibrium force that extends to distances of up to 35 ionic diameters per surface (24, 25). Modeling this force as a diffuse double-layer interaction with a decay length corresponding to the Debye length led to the hypothesis that RTILs can be conceptualized as very weakly dissociated electrolyte "solutions," where the electrostatic screening behavior is dominated by a small population of effectively dissociated ions (24).

However, the molecular mechanism of this apparent ion dissociation in RTILs remained to be explored. Unlike conventional, fully dissociated dilute electrolyte solutions, where the free-ion concentration is independent of temperature and the Debye length only modestly increases with temperature, one would expect the concentration of effectively dissociated ions and Debye length of RTILs, and other highly concentrated electrolytes where ionic aggregation is prominent, to strongly depend on the temperature. For these weakly dissociated electrolytes, increasing the temperature will dissociate ionic aggregates, significantly decreasing the Debye length.

Using the SFA technique, we studied two common aprotic ionic liquids with the bis(trifluorosulfonyl)imide ($[NTf_2]^-$) anion and two different 1-alkyl-3-methylimidazolium cations: $[C_2mim]^+$ and $[C_3mim]^+$ (Fig. 1). Our results suggest that a long-range, monotonic force may be a general feature of the electric double layers formed by RTILs in contact with macroscopic charged surfaces, whenever surface-bound ion layers are unable to fully compensate surface charges. For mica surfaces, we find this long-range force to be in series with a short-range, nonmonotonic "oscillatory" structural force that is in agreement with the nanoscale surface-induced ion ordering identified in previous work on RTILs (17, 20–25). Further, we show that the long-range screening behavior of RTILs can be rationalized via a thermally activated population of either free ions or correlated charge domains, reminiscent of the free electron/hole approximation used in semiconductor physics.

Results and Analysis

Equilibrium Force–Distance Measurements. Force–distance, $F(D)$, measurements were performed using a standard SFA 2000 (26), with resistive heating coils incorporated into the steel SFA housing (Fig. 2). A detailed description of the force and distance measuring methods can be found in ref. 26. Briefly, the top surface was actuated at constant angstroms-per-second displacement rates via a piezoelectric crystal, and the distance between the surfaces, D, was monitored with angstrom-scale resolution through interferometry. The two surfaces move at constant rates when the surfaces are not interacting, and colloidal interaction forces cause

the surfaces to accelerate or decelerate. The deflection of a double-cantilever spring was used to determine the interaction force between the two surfaces at each distance to nanonewton resolution. This procedure enabled us to determine the distances between, and forces across, the surfaces with experimental errors of $F/R = \pm 0.02$ mN/m and $D = \pm 0.2$ nm.

Each SFA experiment was set up with two freshly prepared single-crystalline mica surfaces. $[C_2mim][NTf_2]$ and $[C_3mim][NTf_2]$ were synthesized, purified, dried, and characterized using a previously established procedure for the preparation of electrochemical-grade RTILs (27). The sizes of these $[C_Rmim]^+$ cations and $[NTf_2]^-$ anions (Fig. 1) both exceed the size of the 4-Å radius of K^+ sites on mica surfaces, and mica surfaces develop negative surface potentials (17, 23–25) when exposed to bulk $[C_Rmim][NTf_2]$ RTILs. This negative potential likely develops through a combination of the dissociation of surface-bound K^+ ions present at cleaved mica surfaces, which are then replaced by larger $[C_Rmim]^+$ cations—"crowding" (13)—and/or the overadsorption of $[NTf_2]^-$ anions in the first surface-bound RTIL layer—"overscreening" (13). Our experiments cannot distinguish between these two possibilities, and the actual negative potential of mica surfaces may result from a complex combination of these two mechanisms. The resulting K^+ concentration in the RTILs would be negligible, even if every K^+ ion were to be replaced by $[C_Rmim]^+$ cations.

Forces were measured on approach rates below which dynamic forces are negligible, as ascertained by forces that are independent of approach rates. Representative force–distance profiles, $F(D)$, measured while bringing together two mica surfaces across $[C_2mim][NTf_2]$ and $[C_3mim][NTf_2]$ are shown by the data points in Fig. 3. Attractive forces arising from separating the surfaces more quickly than the extremely long times required for the viscous RTILs to flow back into the interface were measured during retraction of the mica surfaces, even for separation rates as slow as 2 Å/s (Fig. S1). Equilibrium force–distance measurements are the focus of this study.

To increase the sensitivity of our measurements in the long-range regime of the force–distance profiles ($10 < D < 100$ nm), we used surfaces with larger radii (lower curvatures) than the typical 1- to 2-cm-radius surfaces used previously by us and other researchers (23–25). This strategy is similar to using colloid probes in AFM to increase sensitivity of AFM measurements to weak, long-range colloidal forces. The 4- to 5-cm-radius surfaces we used in the majority of these experiments enabled us to increase our sensitivity to colloidal forces by a factor of approximately five relative to our previous measurements, where we used surfaces with R ≈ 1-cm radii (24). This is the case because the force resolution is set by the absolute value of the measured forces, whereas the magnitudes of the long-range double-layer forces scale as F/R, via the Derjaguin approximation (26, 28). The inherent tradeoff to this strategy is that extensive surface deformations (flattening) begin to occur at surface separations $D < 5$ nm with the larger-radius surfaces, limiting the final pressures that we can apply to the strongly surface-bound ion layers. As a result, we cannot fully "force out" all of the ion layers
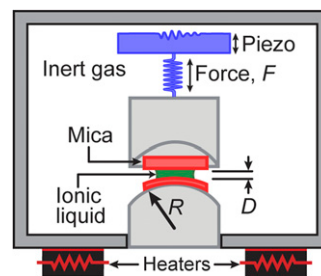

Fig. 2. Schematic of the SFA (26). The temperature was controlled via resistive heaters, and the distance between the two surfaces, D, was defined with respect to the contact of the two mica surfaces in the absence of RTIL, where $D = 0$.
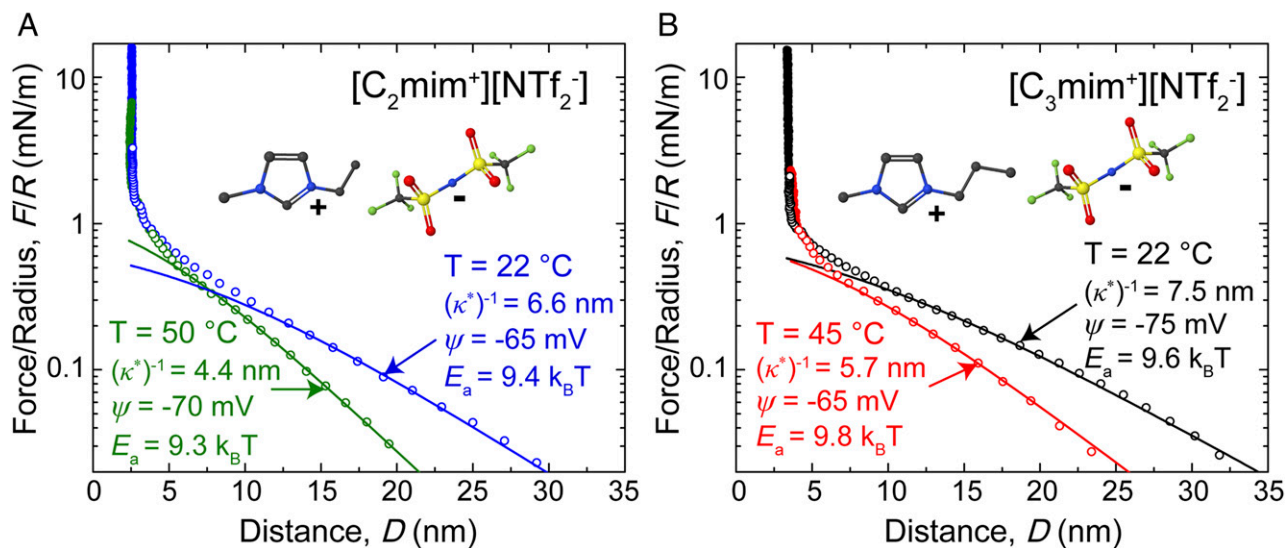
Fig. 3. Representative force–distance profiles measured across (*A*) [C$_2$mim][NTf$_2$] at T = 22 °C (blue data points) and 50 °C (green data points) and (*B*) [C$_3$mim][NTf$_2$] at T = 22 °C (black data points) and 45 °C (red data points). The open circles represent distances where the forces were measured without surface deformations, and the filled circles indicate progressive flattening of the surfaces under increasing loads, where the pressure applied to the bound ion layers stays approximately constant. The solid lines are fitted using the diffuse double-layer interaction potential, Eq. **1**. The interaction potential is plotted for all *D*, but fits were numerically optimized for *D* > 1.5 (κ*)$^{-1}$, as discussed in the text. The parameter values presented on the plot correspond to the fitted parameters of the representative data. The average fitted parameters and SEs are presented in Tables 1 and 2.

to access the entire range of "oscillatory" forces that were the focus of previous studies (21–23).

To ensure consistency with previous studies and to rule out large surface radii as the origin of the monotonic forces we report, we also prepared 1-cm-radius surfaces for a subset of experiments. These experiments exhibited quantitative agreement with the larger radius surfaces in the intermediate ranges of the force–distance profiles (*D* > 5 nm) and enabled us to measure pronounced nonmonotonic forces at surface separations of *D* < 5 nm. Representative results highlighting the short range non-monotonic forces are presented in Figs. S2 and S3.

Analysis of Force–Distance Profiles. The lines plotted in Fig. 3 correspond to fits of a constant potential solution to the linearized Poisson–Boltzmann equation, Eq. **1**, to the asymptotic long-range distance regime of each force profile, *D* > 1.5 (κ*)$^{-1}$, where the equation is well approximated by a simple exponential decay (28, 29):

$$\frac{F}{R} = 2\pi E = \frac{8\pi e^2 n^*}{k_B T \kappa^*} \frac{\psi^2 (1 - \exp(-\kappa^* D))}{\exp(\kappa^* D) - \exp(-\kappa^* D)} \approx \frac{8\pi e^2 n^*}{k_B T \kappa^*} \psi^2 \exp(-\kappa^* D)$$

[1]

$$(\kappa^*)^{-1} \equiv \sqrt{\frac{\varepsilon \varepsilon_0 k_B T}{2 n^* (q^*)^2}},$$

[2]

where $(\kappa^*)^{-1}$ (meters) is the effective Debye length, n^* (meters^{-3}) is the number density of effective charge carriers (free ions or coordinated aggregates of ions that behave as electrostatic monopoles, that is, "quasiparticles"), $q^* = z e$ (coulombs) is the effective carrier charge, $z = 1$ is the carrier valence, ψ (volts) is the diffuse double-layer potential of the mica surfaces, $\varepsilon = 12.3$ for [C$_2$mim][NTf$_2$] and $\varepsilon = 11.6$ for [C$_3$mim][NTf$_2$] is the (measured) low-frequency bulk dielectric permittivity (30), ε_0 (farads per meter) is the vacuum permittivity, T (kelvin) is the temperature, and k$_B$ (joules per kelvin) is the Boltzmann constant. At distances of $D \leq (\kappa^*)^{-1}$, the $F(D)$ profiles deviate from the predictions of mean-field theory and exhibit nonmonotonic "oscillatory" features. The ranges and magnitudes of these

repulsive forces are consistent with previous work that attributed these oscillatory forces to the ordering of the RTIL ions next to charged mica surfaces, with the instabilities corresponding to the abrupt ejection of mixed layers of ions into the reservoir (21–25). Additional discussion of these short-range "oscillatory" forces is presented in *Supporting Information*.

The average values of the fitting parameters obtained from analyzing force–distance profiles measured over multiple independent experiments are presented in Tables 1 and 2. The quoted uncertainties are based on statistical analysis of at least 15 different force profiles for each temperature, with a 95% confidence interval. Forces were also measured at intermediate and higher temperatures than those shown in Fig. 3. The average surface potentials, ψ, and interaction decay lengths, $(\kappa^*)^{-1}$, for all of the experiments are listed Tables 1 and 2, and the raw data used to calculate averages can be found in Table S1 and S2.

Based on the current literature, a mean-field theory describing the distributions of point charges would seem to be incapable of capturing the asymptotic decay behavior of the electric double layers formed by RTILs. Indeed, if every ion is assumed to independently contribute to electrostatic screening (i.e., full "dissociation") then the room-temperature Debye lengths of the [C$_2$mim][NTf$_2$] and [C$_3$mim][NTf$_2$] RTILs used in this study should be on the order of 0.1 Å (calculated with $\varepsilon = 1$–10), which is orders of magnitude smaller than the ionic sizes. However, we propose that the much larger interaction decay lengths that we measure across [C$_2$mim][NTf$_2$] and [C$_3$mim][NTf$_2$], $(\kappa^*)^{-1} = 6.6$ nm and 7.5 nm (room temperature), respectively, are effective Debye lengths, where the effective ionic strength (activity) of the RTILs, n^* (meters^{-3}), substantially differs from the total ionic concentration determined from the RTIL density and molar mass.

The effective Debye lengths that we report always exceed the accepted theoretical Bjerrum length, l_B (5), for [C$_2$mim][NTf$_2$] and [C$_3$mim][NTf$_2$] (4.6 and 4.9 nm at room temperature), Eq. **3**,

$$l_B = \frac{e^2}{4\pi \varepsilon \varepsilon_0 k_B T},$$

[3]

where e (coulombs) is the elementary charge, ε_0 is the vacuum permittivity, ε is the relative permittivity of each RTIL, k$_B$

Table 1. [C$_2$mim][NTf$_2$] average electrostatic parameters (Eqs. 1 and 2) and calculated activation energies (Eq. 4)

Temperature, K	Effective Debye length $(\kappa^*)^{-1}$, nm	Diffuse double-layer potential Ψ, mV	Activation energy E_a, k$_B$T
22	6.7 ± 0.1	90 ± 25	9.4
40	5.7 ± 0.1	100 ± 20	9.6
50	4.3 ± 0.5	90 ± 25	9.3
60	3.4 ± 0.2	100 ± 25	9.1

(joules per kelvin) is the Boltzmann constant, and T (kelvin) is the temperature. l_B is the distance beyond which electrostatic interactions between the free ions or quasiparticle domains are disrupted by thermal energy. Thus, our rescaled mean-field approach fulfills the fundamental requirement that $(\kappa^*)^{-1} > l_B$. For particles and/or length scales that are smaller than l_B, RTILs cannot be modeled using this approach.

As an extension of our recent "dilute electrolyte" analogy (24), we rationalize these measured effective ionic strengths by considering RTILs to behave as thermally dissociable dielectric fluids that are in equilibrium with a Boltzmann-distributed population of either free ions or quasiparticle "ions" (electrostatic monopoles) that exceed an RTIL specific activation energy, E_a. We are not suggesting that the RTIL ions form exclusive ion pairs where each ion coordinates with only one specific counterion; rather, we propose that the strong coulombic interactions between RTIL ions that drive local charge neutrality by causing each cation to be preferentially surrounded by anions (and vice versa) result in the bulk fluid behaving, for large ensembles, as a dipolar network. This picture is consistent with X-ray and neutron reflectivity measurements that independently establish that the strong electrostatic interactions between RTIL ions drive the ions to order into nanoscale bicontinuous cation–anion networks (31, 32). In our model, we use the measured bulk low-frequency dielectric permittivities of the RTILs, ε (30), to account for the dielectric behavior of this network. Thermally activated charge fluctuations, either free ions or correlated charge domains, then behave as (mathematical) point charges (Fig. 4), taking on the role of ions in the traditional Poisson–Boltzmann model for dilute electrolyte solutions.

As an example of the underlying physics, even a simple ion, such as K$^+$, is, in reality, composed of highly correlated charged particles (protons and electrons), with the formal positive charge coming from one missing electron. Nevertheless, K$^+$ ions can be modeled as point charges for length scales (Gaussian surfaces) that are much larger than the angstrom-scale size of K$^+$ ions. For RTILs, the length scales (Gaussian surfaces) over which electrostatic screening in RTILs can be envisioned in terms of point charges need to exceed l_B (Fig. 4). This picture shares conceptual similarities with the "dressed ion" theory of electrolyte solutions (29), an exact statistical mechanical theory that uses charged quasiparticles to model the electrostatic interaction forces between surfaces that are immersed in (nonideal) primitive model electrolyte solutions. However, RTILs have yet to be fully analyzed within this framework.

The physical relevance of viewing bulk RTILs as thermally dissociable dielectric fluids is substantially strengthened by our observation that the measured effective Debye lengths, $(\kappa^*)^{-1}$, decrease as the temperature increases. In the absence of thermally driven ion dissociation, double-layer interactions would increase in range at higher temperatures. Furthermore, several recent theoretical studies proposing that RTILs already behave as highly dissociated (uncorrelated) "electrolytes" at room temperature also appear to predict that the electric double layers formed by RTILs should increase in range with increasing temperature (5, 11). In contrast, our weakly dissociated "dilute electrolyte" model (24) predicts that the double layers formed by RTILs should decrease in range with increasing temperature, as we observe in the current study. Thus, these temperature-dependent measurements provide an unambiguous way to distinguish between the various models.

Calculation of Charge Carrier Activation Energies. Charge carrier activation energies of $E_a = 9.4 \pm 0.3$ k$_B$T for [C$_2$mim][NTf$_2$] and $E_a = 9.7 \pm 0.2$ k$_B$T for [C$_3$mim][NTf$_2$] were calculated from the Boltzmann distribution, Eq. **4**:

$$n^* = n_{tot} \exp\left(\frac{-E_a}{k_B T}\right), \qquad [4]$$

where n^* (meters^{-3}) is the (measured) number density of effective charge carriers, n_{tot} (meters^{-3}) is the total ionic concentration, as determined from the RTIL density and molar mass, and E_a is the charge carrier activation energy. E_a values are reported in units of k$_B$T with T = 295 K. The calculated values of E_a were found to be constant over the 22–75 °C temperature range studied, consistent with an electrostatic screening mechanism that is dominated by thermally excited charge carriers. This temperature independence is not expected to hold for substantially elevated temperatures. For extremely high temperatures (T ≥ 1,500 K), the Bjerrum length would become smaller than the size of the RTIL ions, and n^* will approach the actual molar density of the RTILs. If this temperature limit could be reached without decomposing the RTIL ions, then RTILs should behave as fully "dissociated" ionic melts, as has been observed for high-temperature molten salts (5, 15).

These activation energies of $E_a = 9.4 \pm 0.3$ k$_B$T for [C$_2$mim][NTf$_2$] and $E_a = 9.7 \pm 0.2$ k$_B$T for [C$_3$mim][NTf$_2$] compare well with the activation energy of $E_a = 11$ k$_B$T that we determined for [C$_4$mim][NTf$_2$] (24) and follow the same trend as the dielectric permittivity for this [C$_2$mim][NTf$_2$], [C$_3$mim][NTf$_2$], [C$_4$mim][NTf$_2$] series of RTILs. Using our previous approach of estimating the charge carrier activation energy as the energy required to separate a reference RTIL ion pair within a bulk dielectric fluid also works well for these two RTILs (Eq. **5**):

Table 2. [C$_3$mim][NTf$_2$] average electrostatic parameters (Eqs. 1 and 2) and calculated activation energies (Eq. 4)

Temperature, K	Effective Debye length $(\kappa^*)^{-1}$, nm	Diffuse double-layer potential Ψ, mV	Activation energy E_a, k$_B$T
22	7.4 ± 0.1	72 ± 9	9.6
32	6.6 ± 0.2	75 ± 7	9.7
45	5.5 ± 0.5	66 ± 4	9.8
74	3.5 ± 0.2	50 ± 11	9.5

$$E_a = \Delta\mu^i \approx \frac{\Delta E_d}{\varepsilon}, \qquad [5]$$

where μ^i (joules) is the chemical potential of a reference ion pair, ΔE_d (joules) is the calculated vacuum interaction energy between a $[C_Rmim]^+$ cation and $[NTf_2]^-$ anion averaged over all configurations, and ε corresponds to the measured low-frequency bulk permittivity for each RTIL. For example, the ΔE_d of 132 k_BT (33) and ε of 12.3 (30) for $[C_2mim][NTf_2]$ yields an estimated E_a of 10.7 k_BT, which agrees with the measured E_a of 9.4 k_BT to within 15%. The success of such a simple electrostatic model highlights that electrostatic interactions are the primary determinant of the measured E_a. Further, the simplicity of this molecular-scale model may enable one to quickly estimate, and ultimately tune, the electrostatic screening of properties of RTILs by judiciously balancing bulk dielectric properties with molecular ion pair interaction energies.

Notably, if effectively free "dissociated" ions are taken to be the charge carrier that dominates diffuse layer screening, then these $[C_Rmim][NTf_2]$ RTILs, and by extension other similar aprotic RTILs, would exhibit bulk dissociated ion concentrations of less than 0.1% at room temperature. A similar framework was recently proposed to model the bulk autoionization of pure water (34).

Discussion and Conclusions

The electrostatic screening properties of $[C_2mim][NTf_2]$ and $[C_3mim][NTf_2]$ that we report in the current study are in excellent
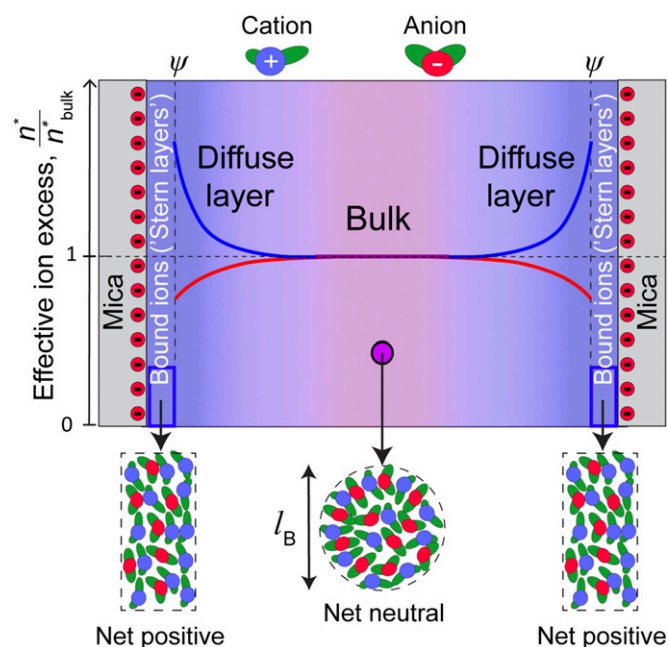
Fig. 4. Electric double layers formed by the RTILs between two surfaces with $D \gg (\kappa^*)^{-1}$. In the "Bound ions ('Stern layers')" region, a portion of the negative surface charge is screened via surface-bound cation-rich ion layers. For $[C_2mim][NTf_2]$ and $[C_3mim][NTf_2]$ at mica surfaces, this region extends approximately two to three ion layers per surface. In the "Diffuse layer" the residual negative potential—the diffuse layer potential, ψ—is screened via a monotonic, steeply decaying concentration of excess positive charge. The blue (cation) and red (anion) lines and blue (positive)-to-purple (neutral) shading approximate the smeared-out excess effective ionic concentrations throughout the diffuse double layer, n^*/n^*_{bulk}. The temperature dependence of the measured decay (Debye) length demonstrates that the charge carriers can be viewed as a Boltzmann-distributed population of effective ions with thermal energy exceeding an RTIL specific activation energy, E_a. The purple circle in the region labeled "Bulk" has a diameter that is approximately the Bjerrum length, l_B (Eq. **3**). RTILs behave as nanoscale, highly charge-ordered (correlated) liquids over distances shorter than l_B.

agreement with our previous study of $[C_4mim][NTf_2]$ in electrochemically active interfaces (24). In both studies, we find that the electric double layers formed by RTILs exhibit a near-surface regime composed of multiple strongly bound layers of ions, where the degree of ordering of the bound ion layers depends on the crystallinity of the confining surfaces. This ubiquitous near-surface regime is in series with a longer-range exponentially decaying diffuse double layer, when the bound ion layers cannot fully screen charged surfaces (Fig. 4). In essence, we propose a Gouy–Chapman–Stern (1) picture of electric double layers in RTILs, where the bound "Stern layer" is several ion layers thick, and the diffuse layer "ions" are either free cations and anions or charged quasiparticles.

A key implication of this study, and of our previous work (24), is that long-range electrostatic interactions should be observed when $[C_Rmim][NTf_2]$ RTILs are confined between (mica) surfaces. In agreement with this prediction, Espinosa-Marzal et al. (25) measured similar long-range electrostatic interactions between two mica surfaces across $[C_2mim]^+$- and $[C_6mim]^+$-based RTILs. In contrast, Perkin et al. (23) studied $[C_4mim][NTf_2]$ and $[C_6mim][NTf_2]$ between symmetric mica surfaces using an SFA but did not report any long-range electrostatic interactions. Perhaps the origin of this discrepancy is that Perkin et al. (23) focused on short-range ion structuring interactions, which would naturally make the simultaneous identification of weaker long-range interactions highly challenging. From our point of view, there may be a monotonic repulsion in the $D > 8$ nm portion of the force–distance profiles presented by Perkin et al. for $[C_4mim][NTf_2]$ in figure 2 of ref. 23.

As noted previously (5), the groundbreaking SFA measurements by Horn and colleagues (21) on an RTIL confined between mica surfaces also reported solely short-range ion structuring interactions. Horn et al. (21) studied the protic RTIL ethylammonium nitrate (EAN), and recent AFM work (35) demonstrates that RTILs with small primary ammonium cations such as EAN bind to mica surfaces with an epitaxial cation spacing that matches the charge-site spacing of the underlying mica substrates. In contrast, the sizes of $[C_Rmim]^+$ cations significantly exceed the 4-Å radius of charge sites on mica surfaces. Thus, we hypothesize that the lack of long-range interactions across EAN arises from an epitaxial compensation of mica surface charges by bound ion layers, an effect that is reminiscent of our observation that $[C_4mim][NTf_2]$ can fully screen negative gold electrodes via bound ion layers (24).

RTILs are typically imagined as strongly dissociated, highly concentrated "electrolytes" when viewed from the perspective of nanoscale simulations (5). In contrast, our experiments portray RTILs as extremely weakly dissociated "electrolytes." We reconcile this apparent contradiction by proposing that the degree of ionic correlations and resultant apparent dissociation of RTIL ions very likely depends on the observed length and time scales of the experiment or computation. An analogous approach was utilized to explain why RTILs seem to simultaneously behave as highly polar liquids ($\varepsilon > 50$) over short distance and time scales but as moderate-polarity liquids ($\varepsilon = 10$–15) over larger distances and longer times (30, 36).

Perhaps the apparently independent diffusion of neighboring ions identified in molecular dynamics simulations (5) only looks independent for the very short length and time scales, and the small number of ions, available to current simulations. Our results reveal that much larger ensembles of ions exhibit complex collective phenomena featuring qualitative differences—in both distance and time—from the behavior identified in nanoscale simulations of ions. Thus, our results should prove useful for the design of energy storage devices, such as electrochemical capacitors (3), where RITLs form double layers at extended surfaces and ionic association strongly affects the stored energy density and conductivity properties of electrochemical devices.

As a practical example, the double-layer capacitance of several RTILs significantly increases with increasing temperature (5), an effect that Lockett et al. (37) explained via the thermal dissociation of neutral ionic aggregates. Our current work supports this

explanation and provides a quantitative framework for estimating the activation energy of ion dissociation in aprotic RTILs, yielding additional insight into the electrochemical performance of RTIL-based capacitors. More broadly, we provide a molecular-scale framework that can be used to design RTILs with carefully tuned degrees of ionic association by judiciously balancing ion pair interaction energies with bulk dielectric properties.

Beyond RTILs, the general physical insight we offer is that the simple picture of dissociation equilibria between neutral ion pairs and dissociated ions that is often invoked to explain moderately concentrated electrolytes (1) needs to be refined for very highly concentrated electrolytes, where distinguishing between specific pairs of ions loses meaning. We instead propose that local excess charge densities fundamentally determine the length scales of electrostatic screening and show that a "dissociation reaction" between effectively neutral ionic networks and either free ions or higher-order correlated charge domains can provide a useful framework for understanding such systems. For example, recent SFA measurements across concentrated aqueous electrolyte solutions (38, 39) establish that the range of electric double-layer interactions increases as the aqueous electrolyte concentrations are increased from 1 to 3 M, but only as long as the electrolyte cation differs from the K^+ ion that is native to mica surfaces. Our results suggest that this trend may be due to the progressive formation of effectively neutral ionic networks involving large numbers of strongly interacting ions. Over the longer term, our results may also prove useful for deciphering how electrostatic interactions maintain such a dominant role near the active sites of proteins, ion channels, and similar self-assembling biological systems (2), where local effective salt concentrations can exceed 10 M.

Materials and Methods

The [C_2mim][NTf_2] and [C_3mim][NTf_2] samples were clear and colorless, and NMR, UV-visible spectroscopy, and electrochemical analysis were used to establish that the RTILs were of electrochemical-grade purity. After synthesis and drying, Karl Fischer titration was used to ensure that the (trace) water content of the [C_2mim][NTf_2] and [C_3mim][NTf_2] RTILs was under 15 ppm, and the samples were stored under vacuum at all times.

Before each SFA experiment, the [C_2mim][NTf_2] and [C_3mim][NTf_2] samples were dried under vacuum at 373 K for at least 72 h. After drying, a droplet of RTIL (50–100 µL) was immediately injected between mica surfaces in a gas-tight SFA under dry nitrogen purge conditions, and the SFA was resealed. All experiments were performed in the presence of a reservoir of the desiccant phosphorous pentoxide (P_2O_5). Each experiment lasted between 24 and 72 h, and the P_2O_5 reservoirs were found to be unsaturated at the conclusion of each experiment.

The temperature was monitored during each experiment via a thermistor with a 0.2 °C tolerance. The thermal expansion of mica was accounted for by calibrating the mica thermal expansion in the absence of RTIL samples. The mica thermal expansion coefficient was found to be 1.5×10^{-5} C^{-1}, in agreement with literature values.

1. Atkins P, de Paula J (2009) *Physical Chemistry* (Oxford Univ Press, Oxford), 7th Ed, pp 252–289.
2. Eisenberg B (2013) Interacting ions in biophysics: Real is not ideal. *Biophys J* 104(9):1849–1866.
3. Simon P, Gogotsi Y (2008) Materials for electrochemical capacitors. *Nat Mater* 7(11):845–854.
4. Alias N, Mohamad AA (2015) Advances of aqueous rechargeable lithium-ion battery: a review. *J Power Sources* 274:237–251.
5. Fedorov MV, Kornyshev AA (2014) Ionic liquids at electrified interfaces. *Chem Rev* 114(5):2978–3036.
6. Welton T (1999) Room-temperature ionic liquids. Solvents for synthesis and catalysis. *Chem Rev* 99(8):2071–2084.
7. Antonietti M, Kuang D, Smarsly B, Zhou Y (2004) Ionic liquids for the convenient synthesis of functional nanoparticles and other inorganic nanostructures. *Angew Chem Int Ed Engl* 43(38):4988–4992.
8. Galiński M, Lewandowski A, Stepniak I (2006) Ionic liquids as electrolytes. *Electrochim Acta* 51(26):5567–5580.
9. Armand M, Endres F, MacFarlane DR, Ohno H, Scrosati B (2009) Ionic-liquid materials for the electrochemical challenges of the future. *Nat Mater* 8(8):621–629.
10. Ye C, Liu W, Chen Y, Yu L (2001) Room-temperature ionic liquids: A novel versatile lubricant. *Chem Commun (Camb)* (21):2244–2245.
11. Lee AA, Vella D, Perkin S, Goriely A (2015) Are room-temperature ionic liquids dilute electrolytes? *J Phys Chem Lett* 6:159–163.
12. Kornyshev AA (2007) Double-layer in ionic liquids: Paradigm change? *J Phys Chem B* 111(20):5545–5557.
13. Bazant MZ, Storey BD, Kornyshev AA (2011) Double layer in ionic liquids: Overscreening versus crowding. *Phys Rev Lett* 106(4):046102.
14. Wu J, Jiang T, Jiang D, Jin Z, Henderson D (2011) A classical density functional theory for interfacial layering of ionic liquids. *Soft Matter* 7:11222–11231.
15. Heyes DM, Clarke JHR (1981) Computer simulation of molten-salt interphases. *J Chem Soc, Faraday Trans II* 77:1089–1100.
16. Merlet C, Salanne M, Rotenberg B, Madden PA (2011) Imidazolium ionic liquid interfaces with vapor and graphite: Interfacial tension and capacitance from coarse-grained molecular simulations. *J Phys Chem C* 115:16613–16618.
17. Zhou H, et al. (2012) Nanoscale perturbations of room temperature ionic liquid structure at charged and uncharged interfaces. *ACS Nano* 6(11):9818–9827.
18. Lynden-Bell RM, Frolov AI, Fedorov MV (2012) Electrode screening by ionic liquids. *Phys Chem Chem Phys* 14(8):2693–2701.
19. Yochelis A (2014) Spatial structure of electrical diffuse layers in highly concentrated electrolytes: A modified Poisson-Nernst-Planck approach. *J Phys Chem C* 118:5716–5724.
20. Mezger M, et al. (2008) Molecular layering of fluorinated ionic liquids at a charged sapphire (0001) surface. *Science* 322(5900):424–428.
21. Horn RG, Evans DF, Ninham BW (1988) Double-layer and solvation forces measured in a molten salt and its mixtures with water. *J Phys Chem* 92:3531–3537.
22. Atkin R, et al. (2011) An in situ STM/AFM and impedance spectroscopy study of the extremely pure 1-butyl-1-methylpyrrolidinium tris(pentafluoroethyl)trifluorophosphate/

23. Perkin S, et al. (2011) Self-assembly in the electrical double layer of ionic liquids. *Chem Commun (Camb)* 47(23):6572–6574.
24. Gebbie MA, et al. (2013) Ionic liquids behave as dilute electrolyte solutions. *Proc Natl Acad Sci USA* 110(24):9674–9679.
25. Espinosa-Marzal RM, Arcifa A, Rossi A, Spencer ND (2014) Microslips to "avalanches" in confined, molecular layers of ionic liquids. *J Phys Chem Lett* 5:179–184.
26. Israelachvili JN, et al. (2010) Recent advances in the surface forces apparatus (SFA) technique. *Rep Prog Phys* 73:036601.
27. Zhou Q, Fitzgerald K, Boyle PD, Henderson WA (2010) Phase behavior and crystalline phases of ionic liquid-lithium salt mixtures with 1-alkyl-3-methylimidazolium salts. *Chem Mater* 22(3):1203–1208.
28. Parsegian VA, Gingell D (1972) On the electrostatic interaction across a salt solution between two bodies bearing unequal charges. *Biophys J* 12(9):1192–1204.
29. Kjellander R, Mitchell DJ (1997) Dressed ion theory for electric double layer structure and interactions; an exact analysis. *Mol Phys* 91(2):173–188.
30. Weingärtner H (2008) Understanding ionic liquids at the molecular level: Facts, problems, and controversies. *Angew Chem Int Ed Engl* 47(4):654–670.
31. Hardacre C, Holbrey JD, Nieuwenhuyzen M, Youngs TGA (2007) Structure and solvation in ionic liquids. *Acc Chem Res* 40(11):1146–1155.
32. Atkin R, Warr GG (2008) The smallest amphiphiles: Nanostructure in protic room-temperature ionic liquids with short alkyl groups. *J Phys Chem B* 112(14):4164–4166.
33. Tsuzuki S, Tokuda H, Hayamizu K, Watanabe M (2005) Magnitude and directionality of interaction in ion pairs of ionic liquids: Relationship with ionic conductivity. *J Phys Chem B* 109(34):16474–16481.
34. Todorova M, Neugebauer J (2014) Extending the concept of defect chemistry from semiconductor physics to electrochemistry. *Phys Rev A* 1:014001.
35. Elbourne A, Voïtchovsky K, Warr GG, Atkin R (2015) Ion structure controls ionic liquid near-surface and interfacial nanostructure. *Chem Sci* 6:527–536.
36. Lui MY, et al. (2011) Salts dissolved in salts: Ionic liquid mixtures. *Chem Sci* 2:1491–1496.
37. Lockett V, Horne M, Sedev R, Rodopoulos T, Ralston J (2010) Differential capacitance of the double layer at the electrode/ionic liquids interface. *Phys Chem Chem Phys* 12(39):12499–12512.
38. Espinosa-Marzal RM, Drobek T, Balmer T, Heuberger MP (2012) Hydrated-ion ordering in electrical double layers. *Phys Chem Chem Phys* 14(17):6085–6093.
39. Baimpos T, Shrestha BR, Raman S, Valtiner M (2014) Effect of interfacial ion structuring on range and magnitude of electric double layer, hydration, and adhesive interactions between mica surfaces in 0.05-3 M Li+ and Cs+ electrolyte solutions. *Langmuir* 30(15):4322–4332.
40. Christenson HK (1983) Experimental measurements of solvation forces in nonpolar liquids. *J Chem Phys* 78(11):6906–6913.
41. Israelachvili JN, Pashley RM (1983) Molecular layering of water at surfaces and origin of repulsive hydration forces. *Nature* 306(17):249–250.
42. Horn RG, Israeleachvili JN (1981) Direct measurement of structural forces between two surfaces in a nonpolar liquid. *J Chem Phys* 75(3):1400–1411.

Au(111) interface: Potential dependent solvation layers and the herringbone reconstruction. *Phys Chem Chem Phys* 13(15):6849–6857.

CHEMISTRY